Optics Communications 332 (2014) 321–326

Contents lists available at ScienceDirect

Optics Communications

journal homepage: www.elsevier.com/locate/optcom

Polarization-dependent terahertz metamaterial absorber with high absorption in two orthogonal directions

Fangrong Hu [a,*], Taobo Zou [a], Baogang Quan [b], Xinlong Xu [b,d,*], Shuhui Bo [c], Tao Chen [a], Li Wang [b], Changzhi Gu [b], Junjie Li [b]

[a] College of Electronic Engineering and automatization, Guilin University of Electronic Technology, Guilin 541004, China
[b] Beijing National Laboratory for Condensed Matter Physics, Institute of Physics, Chinese Academy of Sciences, Beijing 100190, China
[c] Key Laboratory of Photochemical Conversion and Optoelectronic Materials, Technical Institute of Physics and Chemistry, Chinese Academy of Sciences, Beijing 100190, China
[d] Nanobiophotonic Center, State Key Lab Incubation Base of Photoelectric Technology and Functional Materials, and Institute of Photonics & Photon-Technology, Northwest University, Xi'an 710069, China

ARTICLE INFO

Article history:
Received 11 April 2014
Received in revised form
26 May 2014
Accepted 11 June 2014
Available online 24 June 2014

Keywords:
Metamaterial absorber
Terahertz (THz) spectroscopy
High absorption
Polarization-dependent
Orthogonal direction

ABSTRACT

We fabricated a polarization-dependent terahertz (THz) metamaterial absorber consisted of a metal film, a dielectric spacer and a metal pattern layer. The measured absorptivity for *x*-polarized wave is about 0.9 at 1.42 THz, and that for *y*-polarized wave is about 0.87 at 2.15 THz. The full width at half maximum (FWHM) of peaks at 1.42 THz and 2.15 THz are about 0.23 THz and 0.38 THz, respectively. The experimental results are in good agreement with the numerical simulation. In addition, the parameters related to the absorption are presented for deeply understanding the absorption mechanism. Most importantly, these two absorption peaks can be tuned respectively by simply changing the length in *x* and *y* directions. Our results suggest potential applications based on metamaterial absorber, such as THz polarization imaging, selective spectral detection, THz sensing and polarization multiplexing.

1. Introduction

Metamaterials [1] are artificially constructed electromagnetic materials which have unique performance not available in nature. Therefore, they have many potential applications, such as perfect absorbers [2–6], electromagnetic cloaks [7], selective thermal emitters [8] and stealth [9].

Generally, terahertz (THz) wave is defined as the far-infrared (FIR) electromagnetic radiation between 0.1 and 10 THz (1 THz = 10^{12} Hz). In the last two decades, THz technology has developed very quickly due to its special electromagnetic characteristics and potential applications. For example, THz wave can be used to detect and identify many concealed threats, i.e., plastic explosives, illegal drugs, chemical and biological agents [10]. At present, one of the most important issues in THz community is to enhance the sensitivity of THz detectors.

Recently, metamaterials based absorbers working at THz region have attracted more and more attention for their potential applications including THz detecting, sensing and imaging. Since the first THz metamaterials absorber [11] presented in 2008, many types of THz metamaterial absorbers, such as single band [12,13], dual-band [14–18], triple-band [19], multiband [20,21], wideband [22], wide incidence angle [23], and matrix structure [24] THz metamaterials absorbers have been demonstrated.

Despite high absorptivity is achieved, most of the existing THz metamaterial absorbers are polarization-independent or only sensitive to one direction. However, in some application cases, e.g., THz polarization imaging, selective spectral detection, THz sensing and polarization multiplexing, high absorption peaks in two orthogonal directions are very useful and demanded.

In this work, a polarization-dependent THz metamaterial absorber which has high absorption peaks in two orthogonal directions is experimentally demonstrated. The measured high absorption peaks are located at about 1.42 THz for *x*-polarization and 2.15 THz for *y*-polarization, respectively. More interesting, these two absorption peaks can be tuned respectively by simply changing the length in *x* and *y* directions.

2. Structure and design of metamaterial absorber

As shown in Fig. 1, from bottom to top, a single unit cell of the metamaterial absorber consists of silicon substrate, metal film,

* Corresponding authors.
E-mail addresses: hufangrong@sina.com (F. Hu), xlxuphy@nwu.edu.cn (X. Xu).

http://dx.doi.org/10.1016/j.optcom.2014.06.017
0030-4018/

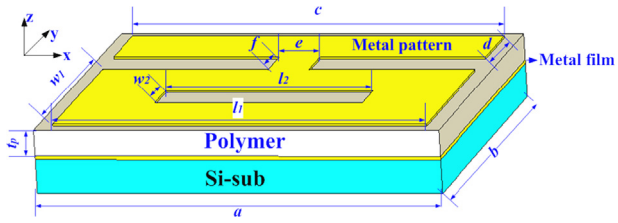

Fig. 1. Unit cell of the metamaterial absorber.

Table 1
Optimized geometries of the unit cell (all units in μm).

a	b	c	d	e	f	l_1	l_2	w_1	w_2	t_p
78	72	72	16	8	9	72	40	31	9	4.2

dielectric spacer (i.e., polymer) and metal pattern layer. The geometrical parameters of the metamaterial absorber, i.e., a, b, c, d, e, f, l_1, l_2, w_1, w_2 and t_p, are all labeled in Fig. 1. Where, a and b are the length and width of the unit cell of the metamaterial absorber, respectively. t_p is the thickness of the spacer, and others are the geometrical parameters of the top metal pattern layer.

In the course of design, a finite-difference time-domain (FDTD) method based commercial software CST Microwave Studio 2011 is used to simulate and optimize the absorption performance of the metamaterial absorber. In the simulation, both the metal film and the metal pattern layer are modeled as lossy gold with electric conductivity $\sigma=4.09\times10^7\ \mathrm{S\ m^{-1}}$ [18]. The dielectric spacer is lossy polymer (i.e., epoxide resin) with an experimental demonstrated a real electrical dielectric constant of $\varepsilon_r=1.4$ and a dielectric loss tangent $\tan\delta=0.04$. Due to the skin depth of the THz wave on the gold film is less than 100 nm, THz wave cannot penetrate the gold film and then the silicon substrate can be ignored in the simulation. The periodic boundary condition is applied in the x and y directions, and an open boundary condition is set in z direction, respectively. The transmission amplitude $S_{2,1}$ and reflection amplitude $S_{1,1}$ can be initially obtained by using frequency domain solver. Then, the absorptivity can be calculated using equation $A=1-|S_{1,1}|^2-|S_{2,1}|^2$. Due to the transmission parameter $S_{2,1}=0$, the absorptivity is simplified as $A=1-|S_{1,1}|^2$. The finally optimized geometries of the unit cell of the metamaterial absorber are listed in Table 1, and the thicknesses of two metal layers are 100 nm.

3. Experiment

The sample was fabricated as follows. Firstly, 5 nm thick Ti, followed by 100 nm thick Au, was deposited on the surface of the silicon substrate. 4.2 μm thick polymer (i.e., epoxide resin) was then spin coated as a dielectric spacer. After that, photolithography was used to define the metallic pattern layer. Lastly, 5 nm thick Ti, followed by 100 nm thick Au, was evaporated, and a metal lift-off process was used to complete the pattern transfer. The photograph of the metamaterial absorber sample is shown in Fig. 2.

The sample is characterized using a commercial THz time domain spectral system, which is made by Zomage Corporation and shown as Fig. 3. In the experiment of reflection test, a smooth copper mirror is used as a reference, and the distance from the back surface of the convex lens to the surface of the reference or the sample is just as the focus of the convex lens as shown in Fig. 3. Vertically polarized THz wave is produced by photoconductor antenna and approximately normally incident on the surface of the reference or the sample, and then reflected. The reflectivity is defined as the reflected power from the surface of the sample

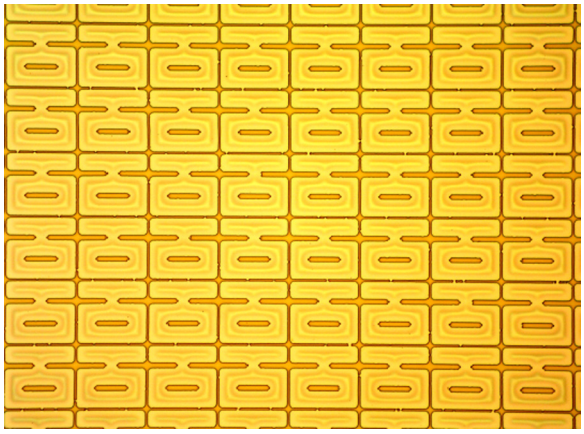

Fig. 2. Photograph of the metamaterial absorber sample.

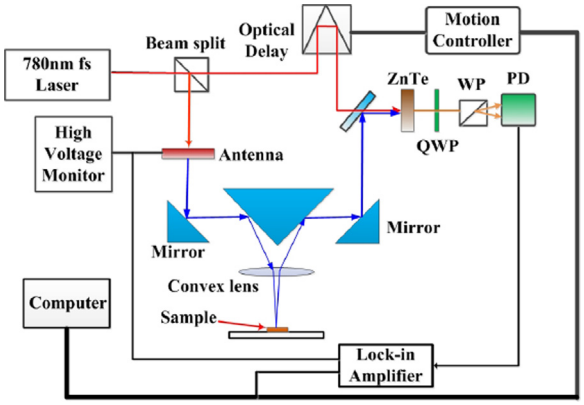

Fig. 3. Test experiment setup.

divided by that from the surface of the reference. Due to the incident THz wave is vertically polarized and cannot be changed, the reflectivity of y-polarization is first tested. And then, the reflectivity of x-polarization is tested by rotating the sample by 90° in the plane. The simulation and the experiment results are plotted in Fig. 4(a) and (b), respectively.

Fig. 4(a) shows that, for x-polarized THz wave, there is a distinct absorption peak at 1.45 THz. When the THz wave turns into y-polarized, the absorption peak shifts to 2.15 THz. The experiment result, as shown in Fig. 4(b), shows that the absorptivities of two peaks are about 0.9 and 0.87, respectively. And the experiment agrees well with the simulation except that low frequency absorption peak shifts from 1.45 THz to 1.42 THz. The measured full width at half maximum (FWHM) of the resonant peaks at 1.42 THz and 2.15 THz are about 0.23 THz and 0.38 THz, respectively. In addition, the relative bandwidths, which defined as the percentage of the FWHM to the corresponding central frequencies, are about 16% and 18%, respectively.

4. Absorption mechanism

Actually, the top metal pattern layer of the metamaterial absorber consists of two sections, i.e., S_1 and S_2, which shown as the inset in Fig. 5. In this figure, dashed lines, i.e., line 1 and line 4, are generated by the metamaterial absorber, whose metal pattern layer only consists of S_1 array. Line 1 is produced by x-polarized wave and line 4 is produced by y-polarized wave, respectively.

At the same time, solid lines, i.e., line 2 and line 3, are generated by the metamaterial absorber whose metal pattern

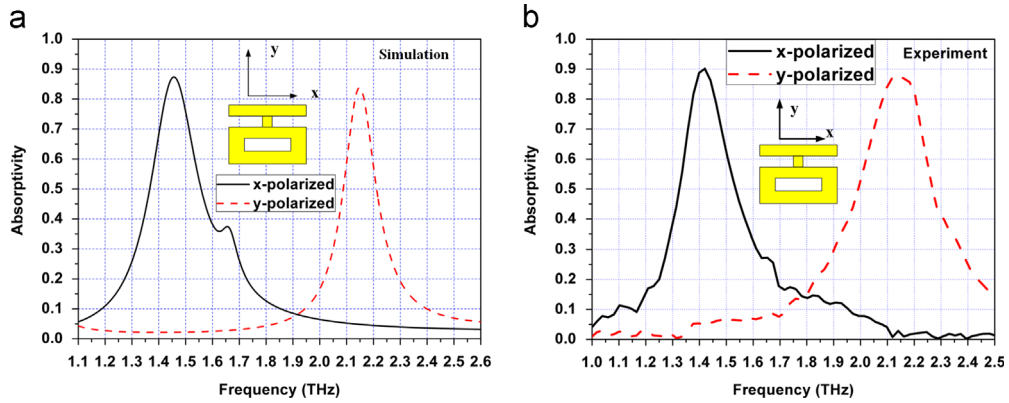

Fig. 4. Absorptivity of metamaterial absorber with simulation (a) and experiment (b) results.

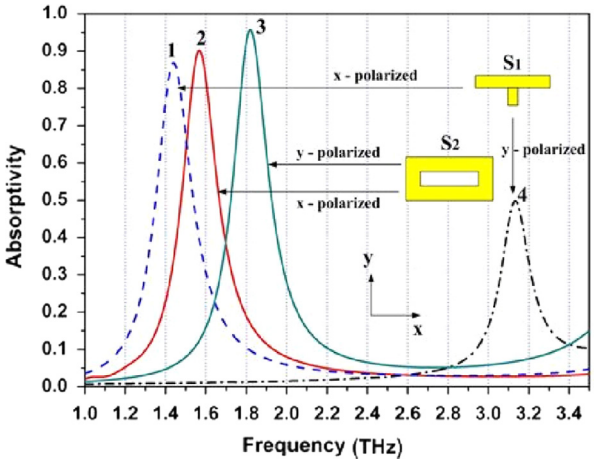

Fig. 5. Simulated absorption spectra of the metamaterial absorber whose top metal pattern only consists of S_1 or S_2 array.

layer only consists of S_2 array. Line 2 is produced by *x*-polarized wave and line 3 is produced by *y*-polarized wave, respectively.

It is easy to see from Fig. 5 that the absorption peaks of those four lines are about 1.42 THz, 1.58 THz, 1.82 THz and 3.12 THz, respectively.

When S_1 and S_2 are merged, new absorption peaks will be produced due to strong electromagnetic coupling between S_1 and S_2. A new absorption peak produced by *x*-polarized wave should locate between 1.42 THz and 1.58 THz, which are produced by S_1 and S_2, respectively. Similarly, another new absorption peak frequency produced by the *y*-polarized wave should be between 1.82 THz and 3.12 THz. For the designed metamaterial absorber, the simulated new absorption peak frequencies are 1.45 THz and 2.15 THz, which are exactly in the frequency range determined by the coupling interaction between S_1 and S_2.

To deeply understand the physics of the absorption, the surface current distributed on the metal film and the metal pattern layer are plotted in Fig. 6.

Fig. 6(a) and (b) show that, for 1.45 THz *x*-polarized wave, the surface current on the metal pattern flows along the direction of the electric field vector, while that of the metal film is reversed. And thus, circulating currents between two metal layers are formed and the magnetic response is excited. Because electric response is produced by top metal pattern layer, and the magnetic response is excited by combining the top metal pattern with the bottom metal film.

Similarly, when *y*-polarized THz wave incidents, three dipoles are produced (shown in Fig. 6(c) and (d)). The absorption peak of 2.15 THz is actually contributed by the coupling interaction between these three dipoles. Since this coupling interaction could dramatically shift the resonant frequency with respect to the isolated dipole.

It should be noted that, as shown in Fig. 6(a), the current oscillate in phase in S_1 and S_2 for *x*-polarization, because the symmetric resonation mode is excited in this case. However, as shown in Fig. 6(c), the current oscillate out-of phase in S_1 and S_2 for *y*-polarization. The reason is that the antisymmetric resonation modes [25] are excited by *y*-polarized incident wave.

In addition, the simulated power loss density of different layers at two absorption peak frequencies is illustrated in Fig. 7.

Fig. 7 indicates that the power is dissipated on the surface of the metal film, in the dielectric spacer and on the bottom surface of the metal pattern. Very little power is dissipated on the top surface of the metal pattern. This can be interpreted by a multi-reflection interference theory [26], because multiple reflections between the bottom metal film and the top metal pattern layer can effectively trap the energy of the incident THz wave in the metamaterial absorber and then cause a high absorptivity.

5. Parametric study of absorption peaks

Generally, the position and the amplitude of every absorption peak are determined by the geometrical and material parameters of the metamaterial absorber. Here, we only discuss five different cases. In each case, only one parameter, e.g. c, l_2, e, ε_r or $\tan\delta$, is changed and the others are kept constant as listed in Table 1 in Section 2. The calculated results are plotted in Fig. 8(a)–(e).

It is easy to know from Fig. 8(a) that the change of the length c only affects the position of the absorption peak produced by *x*-polarized THz wave. The reason is that the circulating currents are produced between the top and the bottom metal layers, and thus, the metamaterial absorber can be equivalent to a *LC* circuit model (as shown in the inset of Fig. 8(a)) [27] with a resonant frequency

$$f = \frac{1}{2\pi\sqrt{LC/2}} \tag{1}$$

where L is the equivalent inductance, and C is the equivalent capacitance of the model. Due to the equivalent inductance L increases with c, it is easy to know from the formula (1) and Fig. 5 that the first resonant absorption peak f_1 (shown in Fig. 5) decreases with c. Consequently, the absorption peak at 1.42 THz will decrease with c as well.

At the same time, Fig. 8(a) shows that the absorption peak at 2.15 THz is independent of the length c. Because this absorption peak is only induced by the antisymmetric resonation shown in Fig. 8(c) and this resonation is insensitive to the length c.

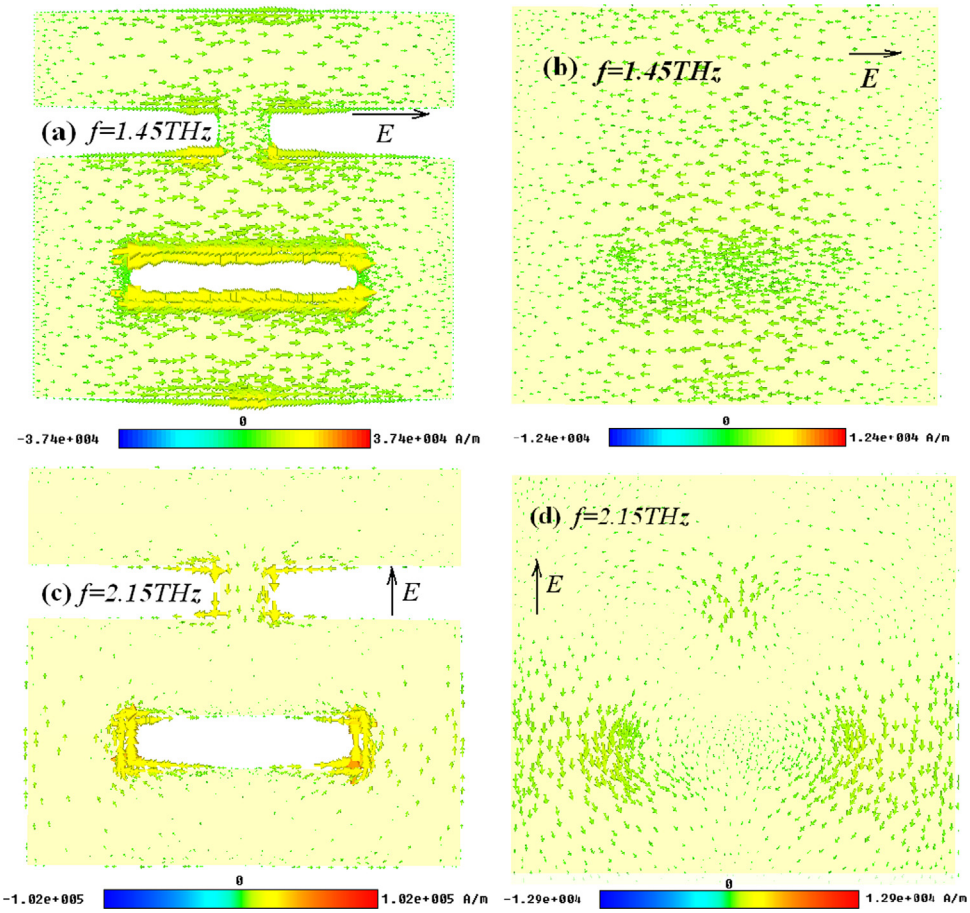

Fig. 6. Simulated surface current distribution on (a) metal pattern at 1.45 THz, (b) metal film at 1.45 THz, (c) metal pattern at 2.15 THz and (d) metal film at 2.15 THz.

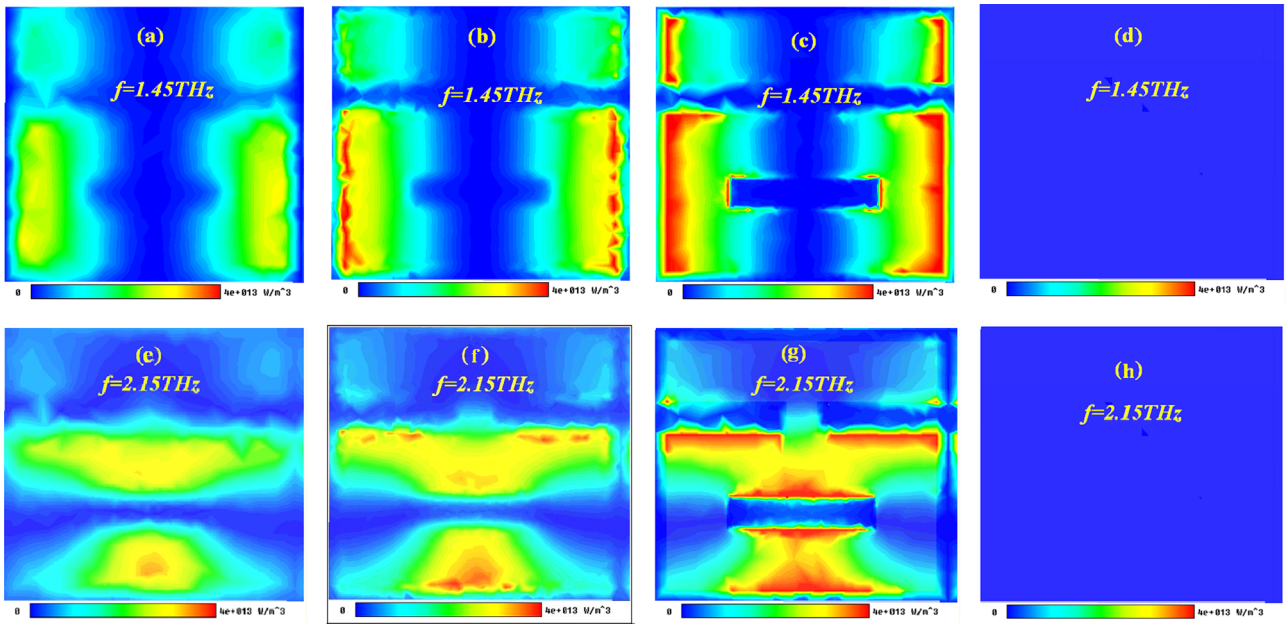

Fig. 7. Simulated power loss density on (a) surface of metal film, (b) middle plane of polymer, (c) bottom surface of metal pattern, (d) top surface of metal pattern at 1.45 THz, (e) surface of metal film, (f) middle plane of polymer, (g) bottom surface of metal pattern and (h) top surface of metal pattern at 2.15 THz.

Fig. 8(b) shows that, for *x*-polarized THz wave, the absorption peak at 1.45 THz is independent of the length l_2. The reason is that the equivalent inductance L of the section S_2 is approximately insensitive to the length l_2 in this case. However, for *y*-polarized incident wave, the absorption peak at 2.15 THz is very sensitive to l_2, and both the position and the amplitude of this absorption peak decrease with l_2. Because, for *y*-polarized THz wave, l_2 only affects the equivalent inductance L of the section S_2 and L increases with l_2. From the formula (1) and Fig. 5, it is easy to know that the third resonant absorption peak f_3 (shown in Fig. 5) decreases with l_2.

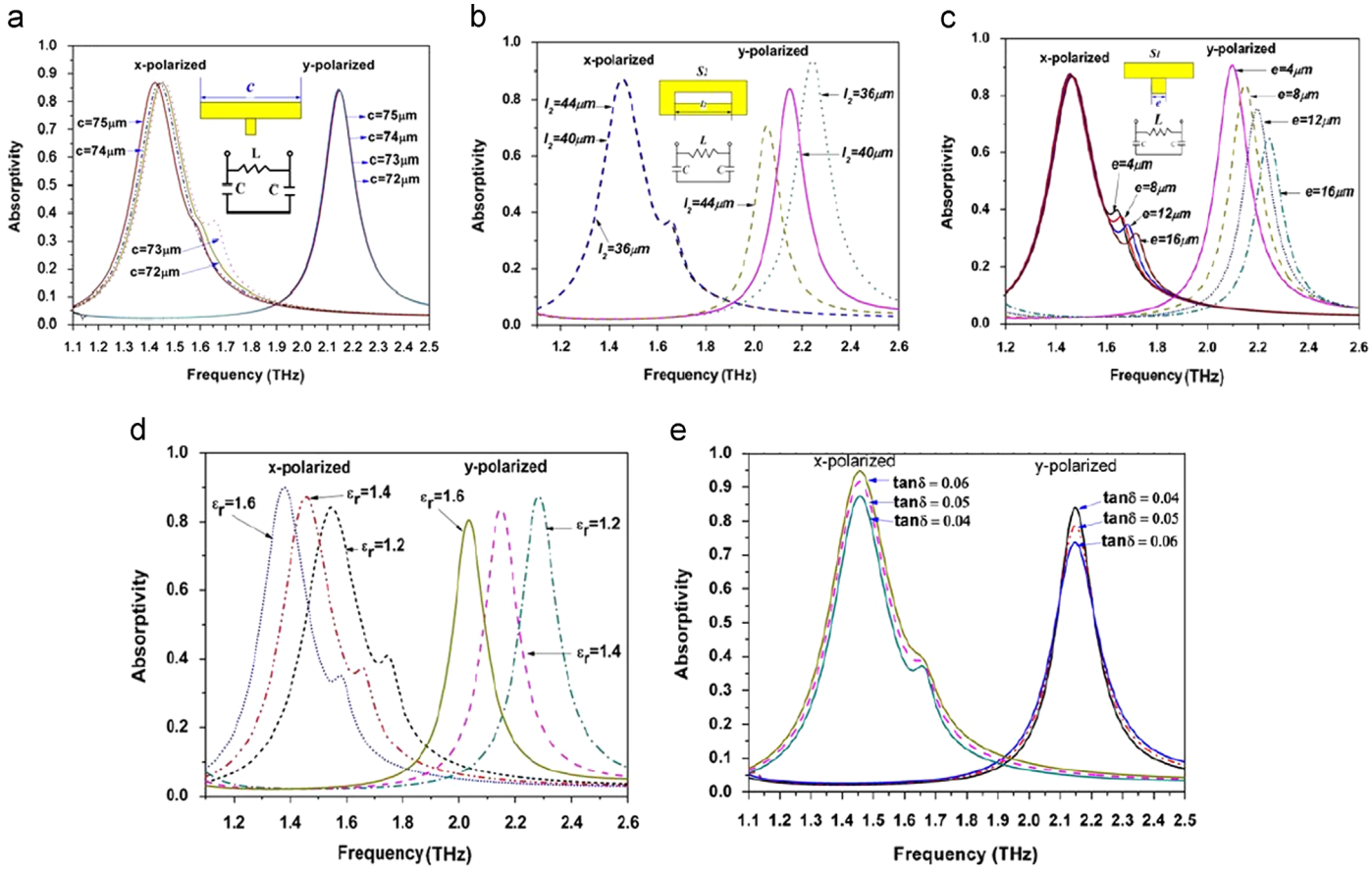

Fig. 8. Absorption peaks affected by (a) length c, (b) length l_2, (c) width e, (d) εr and (e) tan δ.

Consequently, the absorption peak at 2.15 THz will decrease with l_2.

Fig. 8(c) shows that, for x-polarized incident wave, the absorption peak at 1.45 THz does not change with the width e. This is because the width e does not affect the equivalent inductance L of the section S_1 in this case. However, for y-polarized incident THz wave, the position and the amplitude of the absorption peak at 2.15 THz are very sensitive to the width e. The reason is that, the equivalent inductance L of the section S_1 decreases with the width e. It is easy to know from formula (1) that the fourth resonant absorption peak (shown in Fig. 5) increases with e. In addition, for x-polarized THz wave, the small absorption peak appears at about 1.65 THz is also excited by the coupling between the structure of S_1 and S_2. And this peak is mainly determined by the structural parameters of c (see Fig. 8(a)) and e (see Fig. 8(c)).

When the real electrical dielectric constant ε_r increases, two absorption peaks demonstrate redshifts as shown in Fig. 8(d). This is due to large ε_r introduces big capacitance C which is in direct proportion to $\varepsilon_r S/d$. Therefore, it can be deduced from the formula (1) that the resonant frequency f will decrease with ε_r.

Fig. 8(e) shows that the respective positions of the two absorption peaks are nearly independent of the tan δ, but the amplitude of them changes with the tan δ. In addition, the amplitude of the absorption peak at 1.45 THz increases with the tan δ, and that of the other peak at 2.15 THz decreases with the tan δ. These results suggest that we can effectively control the absorptivity of two absorption peaks through optimizing the tan δ, which can be optimized by the chosen polymers. Therefore, it is easy to achieve a desired absorption peak frequency by properly tuning the geometries of the absorber and selecting dielectric spacer.

6. Conclusion

In conclusion, a polarization-dependent THz metamaterial absorber is designed and fabricated. The sample is characterized by measuring the reflection with a THz time domain spectral system. Two intensive absorption peaks are detected at 1.42 THz for x-polarized wave and at 2.15 THz for y-polarized wave, respectively. The most important feature of the absorber is that it is easy to tune cross resonators by simply changing the length in x and y directions. A LC equivalent circuit model is introduced to interpret the influence of structural parameters on the absorption peaks. Moreover, the absorption band can be extended to microwave, infrared and other frequency range by scaling the geometries and changing the spacer material parameters of the metamaterial absorber. Some potential applications of the metamaterial absorber include THz polarization imaging, selective spectral detection, THz sensing and polarization multiplexing.

Acknowledgments

This research is partly supported by the National Natural Science Foundation of China (Nos. 61265005, 61077082, 61101054, 11374240, and 51103175) and the Natural Basic Research Program of China (No. 2009CB930502); partly supported by the foundation from Guangxi Experiment Center of Information Science Guilin University of Electronic Technology (No. 20130101) and the Knowledge Innovation Project of CAS (No. KJCX2-EW-W02); and partly supported by the program (No. YQ14114) from the Key Lab of Guangxi automation test technology and instrument, the innovation project of Guangxi Graduate Education (No. YCSZ2014141),

and the program for innovation research team of Guilin University of Electronic Technology.

References

[1] J.B. Pendry, A.J. Holden, D.J. Robbins, W.J. Stewart, IEEE Trans. Microw. Theory Tech. 47 (1999) 2075.
[2] D.X. Wang, W.Q. Zhu, M.D. Best, J.P. Camden, K.B. Crozier, Sci. Rep. 3 (2013) 2867.
[3] M. Kang, F. Liu, T.F. Li, Q.H. Guo, J.S. Li, J. Chen, Opt. Lett. 38 (2013) 3086.
[4] N.I. Landy, S. Sajuyigbe, J.J. Mock, D.R. Smith, W.J. Padilla, Phys. Rev. Lett. 100 (2008) 207402.
[5] N. Liu, M. Mesch, T. Weiss, M. Hentschel, H. Giessen, Nano Lett. 10 (2010) 2342–2348.
[6] J.M. Hao, J. Wang, X.L. Liu, W.J. Padilla, L. Zhou, M. Qiu, Appl. Phys. Lett. 96 (2010) 251104.
[7] D. Schurig, J.J. Mock, B.J. Justice, S.A. Cummer, J.B. Pendry, A.F. Starr, D.R. Smith, Science 314 (2006) 977.
[8] X.L. Liu, T. Tyler, T. Starr, A.F. Starr, N.M. Jokerst, W.J. Padilla, Phys. Rev. Lett. 107 (2011) 045901.
[9] K. Iwaszczuk, A.C. Strikwerda, K. Fan, X. Zhang, R.D. Averitt, P.U. Jepsen, Opt. Express 20 (2012) 635.
[10] J.F. Federici, B. Schulkin, F. Huang, D. Gary, R. Barat, F. Oliveira, D. Zimdars, Semicond. Sci. Technol. 20 (2005) 266.
[11] H. Tao, N.I. Landy, C.M. Bingham, X. Zhang, R.D. Averitt, W.J. Padilla, Opt. Express 16 (2008) 7181.
[12] N.I. Landy, C.M. Bingham, T. Tyler, N. Jokerst, D.R. Smith, W.J. Padilla, Phys. Rev. B 79 (2009) 125104.
[13] J. Grant, Y. Ma, S. Saha, L.B. Lok, A. Khalid, D.R.S. Cumming, Opt. Lett. 36 (2011) 1524.
[14] Q.Y. Wen, H.W. Zhang, Y.S. Xie, Q.H. Yang, Y.L. Liu, Appl. Phys. Lett. 95 (2009) 241111.
[15] Y. Ma, Q. Chen, J. Grant, S.C. Saha, A. Khalid, D.R.S. Cumming, Opt. Lett. 36 (2011) 945.
[16] X.J. He, Y. Wang, J.M. Wang, T.L. Gui, Prog. Electromagn. Res. 115 (2011) 381.
[17] Y. Wen, W. Ma, J. Bailey, G. Matmon, X. Yu, G. Aeppli, Appl. Opt. 52 (2013) 4536.
[18] H. Tao, C.M. Binghan, D. Pilon, K. Fan, A.C. Strikwerda, D. Shrekenhame, X. Zhang, R.D. Averitt, J. Phys. D: Appl. Phys. 43 (2010) 225102.
[19] X.P. Shen, Y. Yang, Y.Z. Zang, J.Q. Gu, J.G. Han, W.L. Zhang, T.J. Cui, Appl. Phys. Lett. 101 (2012) 154102.
[20] C. Gu, S.B. Qu, Z.B. Pei, Z. Xu, J. Liu, W. Gu, Chin. Phys. B 20 (2011) 017801.
[21] F.R. Hu, L. Wang, B.G. Quan, X.L. Xu, Z. Li, Z.A. Wu, X.C. Pan, J. Phys. D: Appl. Phys. 46 (2013) 195103.
[22] L. Huang, D.R. Chowdhury, S. Ramani, M.T. Reiten, S.N. Luo, A.J. Taylor, H.T. Chen, Opt. Lett. 37 (2012) 154.
[23] H. Tao, C.M. Bingham, A.C. Strikwerda, D. Pilon, D. Shrekenhamer, N.I. Landy, K. Fan, X. Zhang, W.J. Padilla, Phys. Rev. B 78 (2008) 241103.
[24] S.A. Kuznetsov, A.G. Paulish, A.V. Gelfand, P.A. Lazorskiy, V.N. Fedorinin, Prog. Electromagn. Res. 122 (2012) 93.
[25] P. Ding, E.J. Liang, L. Zhang, Q. Zhou, Y.X. Yuan, Phys. Rev. E 79 (2009) 016604.
[26] H.T. Chen, Opt. Express 26 (2012) 7165.
[27] Y.Q. Ye, Y. Jin, S. He, J. Opt. Soc. Am. B 27 (2010) 498.